

Structure of molecular liquids: cavity and bridge functions of the hard spheroid fluid

David L. Cheung,^{1,*} Lucian Anton,^{2,†} Michael P. Allen,^{1,‡} and Andrew J. Masters^{2,§}

¹*Department of Physics and Centre for Scientific Computing
University of Warwick, Coventry, CV4 7AL, UK*

²*School of Chemical Engineering and Analytical Science
University of Manchester, Sackville Street, Manchester, M60 1QD, UK*

We present methodologies for calculating the direct correlation function, $c(1,2)$, the cavity function, $y(1,2)$, and the bridge function, $b(1,2)$, for molecular liquids, from Monte Carlo simulations. As an example we present results for the isotropic hard spheroid fluid with elongation $e = 3$. The simulation data are compared with the results from integral equation theory. In particular, we solve the Percus-Yevick and Hypernetted Chain equations. In addition, we calculate the first two terms in the virial expansion of the bridge function and incorporate this into the closure. At low densities, the bridge functions calculated by theory and from simulation are in good agreement, lending support to the correctness of our numerical procedures. At higher densities, the hypernetted chain results are brought into closer agreement with simulation by incorporating the approximate bridge function, but significant discrepancies remain.

PACS numbers: 61.20.Gy, 61.20.Ja, 05.20.Jj

I. INTRODUCTION

The equilibrium properties of homogeneous fluids of spherical particles have been extensively studied both by theory and simulation and a great deal is now known about the thermodynamic properties and the fluid structure [1, 2]. Simulation has been used to calculate the total and direct correlation functions [3], the cavity function [4, 5] and the bridge function [6, 7, 8]. On the theoretical side, integral equation theory (IET) is now capable of making some very accurate predictions. Percus-Yevick (PY) and Hypernetted Chain (HNC) theories have now been extended, for example, by mixing closures so as to obtain identical virial and compressibility equations of state [9, 10]. An alternative approach has been to incorporate approximate forms for the bridge function in the HNC closure. These may take the form of a low-order virial expansion, a bridge function from a reference fluid or an approximate closure relation [11, 12, 13]. While there is still work to be done, especially perhaps on a fundamental treatment of the bridge function, the foundations are rather solid. As a consequence, one is in a good position to construct good density functionals to describe inhomogeneous fluids. A key ingredient of a density functional is an assumed form for the inhomogeneous direct correlation function. It is clearly reassuring if this quantity reduces to the known homogeneous function in the uniform limit and, for spherically symmetric particles, this is a test one may apply.

The equilibrium properties of isotropic fluids of non-spherical particles are less well-characterised. There are

relatively few simulation studies on the direct correlation function [14] and little data for the cavity or bridge functions have been published (site-site functions have been calculated for hard sphere dimers and water [15, 16, 17] while the first bridge diagram has been calculated for the hard spherocylinder fluid for a number of fixed orientations [18]). The PY and HNC equations have been solved for axially symmetric particles (e.g. hard ellipsoids, hard spherocylinders and truncated hard spheres) and the general conclusion is that HNC is superior to PY for significantly aspherical particles, but that there is still a substantial discrepancy between theory and simulation, especially at high density [19, 20, 21, 22]. There have been some attempts to go beyond HNC. Pospíšil et al. [23] have investigated the use of a modified Verlet-bridge closure and have reported improved results. Singh et al. [24] applied a non-spherical version of the Rogers-Young method of mixing PY and HNC closures, again obtaining results for spheroids in good agreement with simulation. Nevertheless the number of such studies is relatively small and, as yet, we do not have sufficient simulation and theoretical studies to claim a foundation to rival that enjoyed by spherical particles.

In this paper we try to address some of these issues, using Monte Carlo (MC) simulations and IET. On the simulation front, we present methodologies for calculating the direct correlation, cavity and bridge functions for isotropic fluids of axially symmetric particles using advanced MC techniques. These methods are used to calculate the molecular correlation functions for a fluid of hard spheroids with major axis of length a and minor axis of length b . We focus here on an elongation $e = a/b = 3$, and present results for a range of densities in the isotropic phase. IET is adapted for fluids of anisotropic particles using invariant expansions of the correlation functions [25, 26] and efficient numerical algorithms [20, 21, 27, 28, 29, 30]. In particular we use the relaxation method of Ng [31] to provide a robust and

*Electronic address: david.cheung@warwick.ac.uk

†Electronic address: lucian.anton@manchester.ac.uk

‡Electronic address: m.p.allen@warwick.ac.uk

§Electronic address: andrew.masters@manchester.ac.uk

easily-programmable algorithm for numerically solving the integral equations. We also examine some analytical properties of the cavity function for non-spherical hard particles and calculate the first two terms in the virial expansion of the bridge function.

The paper is organised as follows. In section II, we give the basic equations relating the correlation functions studied in this article. Section III describes the simulation methods used for the calculation of the cavity function and bridge function. In Section IV we present some technical details of the numerical solution of the IET using the method of Ng [31] and the Monte Carlo procedure used to compute the bridge diagrams. In Section V the results of simulations and IET are compared and discussed. The general conclusion of our study and some future avenues of work are given in Section VI. Some more technical details of the Monte Carlo algorithm for the calculation of the cavity function are presented in the Appendix.

II. GENERAL FORMALISM

The structure of a fluid may be described at a two-particle level by the total correlation function (TCF) $h(1, 2) = g(1, 2) - 1$ (where $g(1, 2)$ is the pair distribution function) or the direct correlation function (DCF) $c(1, 2)$. These are linked via the Ornstein-Zernike (OZ) equation, which for a homogeneous fluid of axially symmetric molecules is [1, 2]

$$h(1, 2) = c(1, 2) + \frac{\rho}{4\pi} \int d^3 c(1, 3) h(3, 2) \quad (1)$$

where ρ is the number density and, as is traditional, $(i) \rightarrow (\mathbf{r}_i, \mathbf{u}_i)$. Here \mathbf{r}_i denotes the centre of mass position of particle i whilst \mathbf{u}_i represents a unit vector along the particle's symmetry axis.

To determine $h(1, 2)$ and $c(1, 2)$, Eq. (1) is usually supplemented by an approximate closure relation. These take the form

$$c(1, 2) = (1 + h(1, 2))(1 - \exp[\beta V(1, 2)]) \quad \text{PY} \quad (2)$$

$$c(1, 2) = h(1, 2) - \log[1 + h(1, 2)] - \beta V(1, 2) \quad \text{HNC} \quad (3)$$

where $V(1, 2)$ is the intermolecular potential and $\beta = 1/k_B T$.

The exact closure relation can be written as follows [1]

$$y(1, 2) = \exp\{h(1, 2) - c(1, 2) + b(1, 2)\} \quad (4)$$

where $b(1, 2)$ is the bridge function and $y(1, 2)$ is the cavity or background correlation function defined by the relation:

$$y(1, 2) = g(1, 2) \exp[\beta V(1, 2)] \quad (5)$$

Eq. (4) may be regarded as a definition of $b(1, 2)$ and the approximate closure relations may be regarded as approximations to the unknown $b(1, 2)$. In particular, the PY and HNC closures, Eqs. (2),(3) respectively, correspond to

$$b(1, 2) = \eta(1, 2) - \log(1 + \eta(1, 2)) \quad \text{PY} \quad (6a)$$

$$b(1, 2) = 0 \quad \text{HNC} \quad (6b)$$

where $\eta(1, 2) = h(1, 2) - c(1, 2)$.

The bridge function may be expressed as a virial expansion

$$b(1, 2) = \sum_{n \geq 2} \rho^n \mathfrak{B}_n(1, 2) ,$$

where $\mathfrak{B}_n(1, 2)$ are the bridge diagrams. In principle, this provides a route for the exact calculation of the bridge function, but in practice it is only feasible to calculate low-order terms, as has been done for hard spheres [12, 13]. In this paper we use the two lowest-order estimates of the bridge function for hard spheroids

$$b_2(1, 2) = \rho^2 \mathfrak{B}_2(1, 2) \quad \text{HNC+B2} \quad (6c)$$

$$b_3(1, 2) = \rho^2 \mathfrak{B}_2(1, 2) + \rho^3 \mathfrak{B}_3(1, 2) \quad \text{HNC+B3} \quad (6d)$$

to extend the HNC closure relation. In this paper we investigate all four closure relations, i.e. Eq. (4) with the bridge function specified by one of Eqs. (6a)–(6d).

The numerical solution of the integral equation and MC calculation are based upon the expansion of two-particle functions in a basis set of rotational invariants [2, 25]:

$$F(1, 2) = \sum_{mn\ell} F^{mn\ell}(r) \Phi^{mn\ell}(\mathbf{u}_1, \mathbf{u}_2, \mathbf{u}_r) , \quad (7)$$

$$\Phi^{mn\ell}(\mathbf{u}_1, \mathbf{u}_2, \mathbf{u}_r) = 4\pi \sum_{\chi_1 \chi_2 \chi_r} \begin{pmatrix} m & n & \ell \\ \chi_1 & \chi_2 & \chi_r \end{pmatrix} \times Y_{m\chi_1}(\mathbf{u}_1) Y_{n\chi_2}(\mathbf{u}_2) C_{\ell\chi_r}(\mathbf{u}_r) , \quad (8)$$

where r is the intermolecular distance; \mathbf{u}_r is a unit vector along the intermolecular vector, $\mathbf{u}_1, \mathbf{u}_2$ are the orientations of the molecules in a given system of coordinates ('laboratory frame'), $Y_{m\chi}(\mathbf{u})$ are the spherical harmonics functions, $C_{m\chi}(\mathbf{u}) = (4\pi/(2m+1))^{1/2} Y_{m\chi}(\mathbf{u})$ and

$$\begin{pmatrix} m & n & \ell \\ \chi_1 & \chi_2 & \chi_r \end{pmatrix}$$

are the standard $3j$ symbols.

Some quantities of interest are easier to compute in a system of coordinates whose z -axis lies along the intermolecular vector ('molecular frame'). The expansion in the molecular frame has the form:

$$F(1, 2) = 4\pi \sum_{mn\chi} F_{mn\chi}(r) Y_{m\chi}(\tilde{\mathbf{u}}_1) Y_{n\bar{\chi}}(\tilde{\mathbf{u}}_2) , \quad (9)$$

where $\bar{\chi} = -\chi$. The two sets of coefficients are connected through the χ -transform and its inverse:

$$F_{mn\chi}(r) = \sum_{\ell} \begin{pmatrix} m & n & \ell \\ \chi & \bar{\chi} & 0 \end{pmatrix} F^{mn\ell}(r) \quad (10a)$$

$$F^{mn\ell}(r) = (2\ell + 1) \sum_{\chi} \begin{pmatrix} m & n & \ell \\ \chi & \bar{\chi} & 0 \end{pmatrix} F_{mn\chi}(r). \quad (10b)$$

III. SIMULATION METHOD

A. Direct correlation function

The total correlation function may be determined directly from simulation through the pair distribution function $g(1, 2)$. The spherical harmonic coefficients are determined as usual from [32]

$$g_{mn\chi}(r) = 4\pi g_{000}(r) \langle Y_{m\chi}^*(\mathbf{u}_1) Y_{n\bar{\chi}}^*(\mathbf{u}_2) \rangle_r, \quad (11)$$

where $Y_{m\chi}(\mathbf{u})$ is a spherical harmonic, $\bar{\chi} = -\chi$, $g_{000}(r)$ is the pair distribution function of the particle centres, and the angled brackets denote an average over all molecules in the shell $[r, r + \delta r]$. These coefficients are defined in the molecular frame described in Section II [2]. From Eq. (11) it follows that $h_{mn\chi}(r) = g_{mn\chi}(r) - \delta_{m0}\delta_{n0}\delta_{\chi 0}$.

The direct correlation function may be found from the measured total correlation function in two ways. In reciprocal space, using the molecular frame expansion, the Ornstein-Zernike equation becomes

$$\tilde{h}_{mn\chi}(k) = \tilde{c}_{mn\chi}(k) + (-1)^x \rho \sum_j \tilde{h}_{mj\chi}(k) \tilde{c}_{jn\chi}(k) \quad (12)$$

where $\tilde{f}(k)$ is the (three-dimensional) Fourier transform of a function $f(r)$. The structure of this equation with respect to the first two indices leads to a matrix notation

$$\tilde{\mathbf{H}}_{\chi}(k) = \tilde{\mathbf{C}}_{\chi}(k) + (-1)^x \rho \tilde{\mathbf{H}}_{\chi}(k) \tilde{\mathbf{C}}_{\chi}(k). \quad (13)$$

$c(1, 2)$ may also be obtained via a real-space factorization [2, 33, 34]. It is possible to write

$$r\hat{\mathbf{C}}_{\chi}(r) = -\mathbf{Q}'_{\chi}(r) + 2\pi(-1)^x \rho \int_r^R ds \mathbf{Q}'_{\chi}(s) \mathbf{Q}_{\chi}^T(s-r) \quad (14a)$$

$$r\hat{\mathbf{H}}_{\chi}(r) = -\mathbf{Q}'_{\chi}(r) + 2\pi(-1)^x \rho \int_0^R ds (r-s) \hat{\mathbf{H}}'_{\chi}(r-s) \mathbf{Q}_{\chi}(s) \quad (14b)$$

where the new matrix $\mathbf{Q}_{\chi}(r)$ has been introduced, $\mathbf{Q}'_{\chi}(r) = d\mathbf{Q}_{\chi}(r)/dr$, and $\mathbf{Q}_{\chi}^T(r)$ is the transpose of $\mathbf{Q}_{\chi}(r)$.

The so-called ‘hat’ transform giving the functions $\hat{\mathbf{H}}_{\chi}$, $\hat{\mathbf{C}}_{\chi}$, that appear in Eqs. (14) is defined in the laboratory frame

$$\hat{f}^{mn\ell}(r) = f^{mn\ell}(r) - \int_r^{\infty} ds s^{-1} f^{mn\ell}(s) P_{\ell}^e(r/s) \quad (15)$$

where $P_{\ell}^e(x) = x^{-1} dP_{\ell}(x)/dx$ and $P_{\ell}(x)$ are Legendre polynomials. A χ -transform, Eq. (10a), then converts the functions to the required molecular frame. It is assumed that a separation R exists such that $\mathbf{Q}_{\chi}(r) = 0$ and $\mathbf{C}_{\chi}(r) = 0$ for all $r > R$. Equation (14b) is solved iteratively to find $\mathbf{Q}_{\chi}(r)$ from the functions $\mathbf{H}_{\chi}(r)$ determined in the simulation. Once this procedure has converged, Eq. (14a) is used to determine $\hat{\mathbf{C}}_{\chi}(r)$. At very small r this involves the difference between two large quantities possibly leading to numerical difficulties. These may be avoided by a procedure outlined previously [14], finding $\hat{\mathbf{C}}_{\chi}(0)$ from

$$\hat{\mathbf{C}}_{\chi}(0) - \hat{\mathbf{H}}_{\chi}(0) = (-1)^x 2\pi\rho \left\{ \left(\int_0^R dr r \hat{\mathbf{H}}_{\chi}(r) \mathbf{Q}'_{\chi}(r) - \mathbf{Q}'_{\chi}(r) \mathbf{Q}_{\chi}^T(r) \right) - \mathbf{Q}_{\chi}(0) \mathbf{Q}_{\chi}^T(0) \right\} \quad (16)$$

and the $\hat{\mathbf{C}}_{\chi}(r)$ for $r \rightarrow 0$ are then determined by interpolation.

B. Cavity correlation function

There are two methods for the calculation of the cavity function, Eq. (5), either by a direct simulation of two non-interacting cavity particles [4] or through the test-particle method based on Henderson’s equation [35]. The first of these methods is more useful for large cavity separations while the second is better as $r \rightarrow 0$.

1. Direct simulation method

The direct simulation method follows from the observation that for the hard particle fluid, the cavity function may be identified as the pair distribution function for a pair of non-interacting cavities [36]. In a MC simulation it is convenient to constrain the two cavities to be within a given range of separations r_{12} . Even so, in a normal MC simulation the probability distribution $P_{\text{cav}}(1, 2)$ is likely to vary rapidly with separation r_{12} , leading to poor sampling in the regions where the function is relatively small. To circumvent this problem, the umbrella sampling technique is employed [37]. The r -separation of the cavities is divided into a set of overlapping windows. Within each window a weight function $w(r_{12})$ is introduced into the Monte Carlo moves; this function is iteratively refined so as to produce a flat sampled probability distribution. This weight may be subsequently removed to give the true probability distribution for each window and the full distribution is recovered using the self-consistent histogram method [38].

The cavity function is, to within a multiplicative constant, equal to $P_{\text{cav}}(1, 2)/r_{12}^2$. When the cavity particles

are constrained this constant cannot be determined directly [6]. However it may be found by enforcing the condition that $y(1, 2) = 1 + h(1, 2)$ when outside the overlap region [4].

For this scheme to be effective a good choice of the weighting function is needed. For hard spheres a good choice proved to be an analytic approximation to $y(r)$ [4]. Here we employ a more general method based on the Wang-Landau method [39, 40]. Briefly, this is an iterative method that updates an initial guess to the weight function using a decreasing modification factor. Full details are given in the appendix. The implementation used here is similar in spirit to the extended density of states method (EDOS) [41, 42]. The spherical harmonics coefficients $y_{mn\chi}(r)$ are found in the same way as those for the pair distribution function $g_{mn\chi}(r)$.

2. Test particle method

In the canonical ensemble, Henderson's equation for a system containing N molecules may be written [6]

$$y(0, 1) = \exp[\beta\mu_{\text{ex}}] \times \left\langle \exp\left(-\sum_{j \geq 2}^N \beta(V(0, j))\right) \right\rangle_{N, V, T}, \quad (17)$$

where μ_{ex} is the excess chemical potential and the angled brackets denote an ensemble average over particles $1, \dots, N$. The term in the angled brackets corresponds to the Boltzmann factor of a molecule 0 with the interaction with another molecule 1 neglected. This may intuitively be equated to a fluid consisting of 2 non-interacting cavities and $N - 1$ other molecules. Additionally this is also equivalent to the calculation of the acceptance criterion in a Metropolis MC simulation - the interaction between a hypothetical molecule with position \mathbf{r}_0 and orientation \mathbf{u}_0 and every molecule in the system apart from 1 is the quantity that is calculated when an attempt is made to move molecule 1 to position \mathbf{r}_0 and orientation \mathbf{u}_0 . So as any molecule in the system may be labelled 1 the quantity in the angled brackets in Eq. (17) is calculated for every attempted MC move. This fact has been used in previous studies of atomic fluids [6, 7] allowing the calculation of $y(0, 1)$ at essentially no extra cost. However, for molecular fluids, where the maximum angular displacement in a Monte Carlo simulation may be much smaller than 2π , this would lead to poor sampling of the angular dependence $y(0, 1)$. Hence the calculation of $y(0, 1)$ proceeds by inserting a number of test particles (labelled 0) in the vicinity of each molecule in the simulation (labelled 1). The Boltzmann factor (neglecting the interaction between 0 and 1) is then calculated. For hard molecules, as in the present case, this is simply 0 if the test particle overlaps with any other molecule (excluding molecule 1) or 1 if there are no overlaps.

The spherical harmonic coefficients $y_{mn\chi}(r)$ are given by

$$y_{mn\chi}(r) = (4\pi)^{-1} \int d\mathbf{u}_0 d\mathbf{u}_1 y(0, 1) Y_{m\chi}^*(\mathbf{u}_0) Y_{n\chi}^*(\mathbf{u}_1) \\ = (4\pi)^{-1} \exp[\beta\mu_{\text{ex}}] \left\langle \exp\left(-\sum_{j \geq 2}^N \beta V(0, j)\right) \right. \\ \left. \times Y_{m\chi}^*(\mathbf{u}_0) Y_{n\chi}^*(\mathbf{u}_1) \right\rangle_r, \quad (18)$$

where the angled brackets denote averages over test particle insertions in the range $[r, r + \delta r]$.

C. Bridge function

Once spherical harmonic expansions for $h(1, 2)$, $c(1, 2)$ and $y(1, 2)$ have been determined, the final step is to invert Eq. (4) for $b(1, 2)$. While the presence of the exponential on the right hand side of Eq. (4) is troublesome for the spherical harmonics expansions, it may be easily circumvented [19]. Taking the logarithm and differentiating Eq. (4) with respect to r gives

$$\frac{\partial y(1, 2)}{\partial r} = y(1, 2) \left[\frac{\partial h(1, 2)}{\partial r} - \frac{\partial c(1, 2)}{\partial r} + \frac{\partial b(1, 2)}{\partial r} \right]. \quad (19)$$

Inserting the spherical harmonic expansions of the pair functions and integrating over angles gives[2]

$$\frac{dy_{mn\chi}(r)}{dr} = 4\pi \sum_{\substack{m'n'\chi' \\ m''n''\chi''}} \Gamma_{\chi\chi'\chi''}^{mm'm''} \Gamma_{\bar{\chi}\bar{\chi}'\bar{\chi}''}^{nn'n''} y_{m''n''\chi''}(r) \\ \times \frac{d}{dr} [h_{m'n'\chi'}(r) - c_{m'n'\chi'}(r) + b_{m'n'\chi'}(r)] \quad (20)$$

where

$$\Gamma_{\chi\chi'\chi''}^{mm'm''} = \int d\mathbf{u} Y_{m\chi}^*(\mathbf{u}) Y_{m'\chi'}(\mathbf{u}) Y_{m''\chi''}(\mathbf{u}) \\ = \sqrt{\frac{(2m'+1)(2m''+1)}{4\pi(2m+1)}} C(m'', m', m; 0, 0, 0) \\ \times C(m'', m', m; \chi'', \chi', \chi), \quad (21)$$

and where $C(m'', m', m; \chi'', \chi', \chi)$ are Clebsch-Gordan coefficients. Eq. (20) can be solved using standard numerical methods [43] for the derivatives $db_{mn\chi}(r)/dr$, and these are integrated numerically to give the bridge function components $b_{mn\chi}(r)$.

D. Simulated system

The simulated system consists of a fluid of hard prolate spheroids of elongation $e = a/b = 3$. This is a common model for molecular fluids and liquid crystals and

along with similar models such as hard spherocylinders has been well studied [44].

For the calculation of $h(1,2)$, systems of 2048 molecules were simulated using constant NVT MC simulations. Data for the calculation of $h(1,2)$ were gathered every 500 MC sweeps (each sweep is on average 1 attempted translation and 1 attempted rotation per molecule) over a total of 5×10^5 MC sweeps. The $c_{mn\chi}(r)$ coefficients were then calculated from the $h_{mn\chi}(r)$ coefficients following Sec. III A. The spherical harmonics expansions for the pair functions were truncated at $m_{\max} = n_{\max} = 8$ and the grid spacing $\delta r = 0.01b$.

For the calculation of $y(1,2)$, systems of 512 molecules, including 2 cavity molecules, were simulated (smaller systems are sufficient for the calculation of $y(1,2)$ as its long-range behaviour is identical to $h(1,2)$). The r separation between the cavity particles was split into overlapping windows covering $r/b = [0.03, 0.50]$, $[0.20, 1.20]$, $[1.00, 2.00]$, $[1.80, 2.80]$, and $[2.60, 3.60]$. In each window the weight function was determined over at least 15 iterations (see appendix for details). Once the final weight function was determined, $y(1,2)$ data were gathered over a total of 2×10^7 MC sweeps. Error estimates were made by splitting this into 4 subruns. $y(1,2)$ was calculated for the region $r/b = [0, 0.15]$ using the test particle insertion method (Sec. III B 2). $h(1,2)$ and $y(1,2)$ have been calculated at reduced densities $\rho^* = \rho/\rho_{\text{cp}} = 0.10, 0.20, 0.30, 0.40, 0.50$ where $\rho_{\text{cp}} = \sqrt{2}/(ab^2)$ is the close-packed density.

IV. INTEGRAL EQUATION THEORY

To solve the integral equations in the isotropic phase we have used the standard rotationally invariant decomposition of the angular part of the correlation functions as discussed in detail in Refs. [20, 27]. The solution is calculated iteratively with the help of the method of Ng [31] that yields fast convergence even at densities close to those where no real solution exists.

We describe in short the Ng method as applied to the hard spheroid fluid. An iteration step in the Ng method is done using as input a linear combination of the p functions obtained in the p previous steps. The coefficients of the linear combination are calculated from a smallest displacement condition.

An iteration has the generic form

$$f_{i+1}(1,2) = \mathcal{O}[t_i(1,2)] \quad (22)$$

$$\text{with } t_i(1,2) = f_i(1,2) - \sum_{m=1}^p \alpha_{i,m} \Delta f_{i,m}(1,2) \quad (23)$$

where $\mathcal{O}[f]$ is the iteration operator, $f_i(1,2)$ is the i^{th} iteration result and $\Delta f_{i,m}(1,2) = f_i(1,2) - f_{i-m}(1,2)$. At each iteration step the scalars $\alpha_{i,m}$ are computed from the minimum condition of the following functional:

$$\int d2 [f_{i+1}(1,2) - t_i(1,2)]^2. \quad (24)$$

Close to the solution we assume that the differences $\Delta f_{i,m}(1,2)$ are small and we expand Eq. (22) up to the first order:

$$\begin{aligned} \mathcal{O}[f_i(1,2) - \sum_{m=1}^p \alpha_{i,m} \Delta f_{i,m}(1,2)] \\ \approx \mathcal{O}[f_i(1,2)] - \sum_{m=1}^p \alpha_{i,m} \frac{\partial \mathcal{O}[f_i(1,2)]}{\partial f_i(1,2)} \Delta f_{i,m}(1,2). \end{aligned} \quad (25)$$

The coefficients $\alpha_{i,m}$ that satisfy the approximated minimum condition, Eq. (24), are the solutions of a linear system of equations

$$\sum_{m=1}^p a_{km} \alpha_{i,m} = b_k, \quad k = 1 \dots p, \quad (26)$$

where the coefficients a_{km} and b_k are determined from the following equations:

$$a_{km} = \int d2 \delta \mathcal{O}[f_i(1,2)]_k \delta \mathcal{O}[f_i(1,2)]_m \quad (27)$$

$$b_k = \int d2 (\mathcal{O}[f_i(1,2)] - f_i(1,2)) \delta \mathcal{O}[f_i(1,2)]_k, \quad (28)$$

and

$$\delta \mathcal{O}[f_i(1,2)]_k = \frac{\partial \mathcal{O}[f_i(1,2)]}{\partial f_i(1,2)} \Delta f_{i,k}(1,2).$$

In our case the nonlinear operator $\mathcal{O}[\cdot]$ has the form [20]

$$\mathcal{O}[\eta] = \lambda(1,2)(-1 - \eta(1,2)) + (1 - \lambda(1,2))c_{\text{cl}}(1,2), \quad (29)$$

where $\lambda(1,2)$ has the value 1 if spheroids 1 and 2 overlap and the value 0 if they do not. $c_{\text{cl}}(1,2)$ is given by

$$0 \quad \text{PY} \quad (30a)$$

$$\exp(\eta(1,2)) - \eta(1,2) - 1 \quad \text{HNC} \quad (30b)$$

$$\exp(\eta(1,2) + b_2(1,2)) - \eta(1,2) - 1 \quad \text{HNC+B2} \quad (30c)$$

$$\exp(\eta(1,2) + b_3(1,2)) - \eta(1,2) - 1 \quad \text{HNC+B3} \quad (30d)$$

corresponding to the closure relations of Eqs. (6).

We mention that the indirect correlation function, $\eta(1,2) = h(1,2) - c(1,2)$, that appears in Eqs. (29), (30) is computed at each iteration step from the OZ equation, and the expansion (25) is performed with the function $\eta(1,2)$.

The algorithm is written using the angular components of the operator $\mathcal{O}[\cdot]$, Eq. (29), and of the correlation functions $c(1,2)$, $\eta(1,2)$ as described in full detail in Ref. [20].

In the numerical calculation, the expansion in rotational invariants of the correlation functions, Eq. (7), is truncated at $m_{\max} = n_{\max} = 8$ and all non-zero components consistent with this truncation are kept. The integral equation was discretized on a grid in steps of $0.01b$.

The first- and second-order bridge diagrams were computed using an extension of the Monte Carlo methods described by Ree and Hoover [45, 46]. The first step was to convert the diagrams from Ref. [12], given in terms of Mayer f -bonds, into Ree-Hoover diagrams, where field points are connected either by an f -bond or by an e -bond, where $e = 1 + f$. The overall bridge function is obtained from a weighted sum of these Ree-Hoover diagrams. Particle 1 is placed at the origin with its symmetry axis along the z axis, and a second particle is placed at random so that it overlaps the first particle. A third particle is similarly randomly placed to overlap the second particle and so on. When calculating the first set of bridge diagrams, a chain of four such particles is generated. The second set of bridge diagrams require a five-particle chain. The overlaps between all pairs of particles are checked. If the configuration corresponds to one of the Ree-Hoover bridge diagrams, then the separation between the two end particles of the chain is calculated, ready for accumulation as a histogram. To obtain the angular expansion coefficients, the Ree-Hoover weighting is multiplied by the spherical harmonic product $Y_{m\chi}^*(\mathbf{u}_1)Y_{n\bar{\chi}}^*(\mathbf{u}_2)$, where the unit vectors are expressed relative to the vector joining the two end particles of the chain (1 and 2). The components of the bridge diagrams are thus in the molecular frame. After a sufficient number of Monte Carlo configurations have been generated, N_{conf} , the final results for the bridge function are obtained by normalising the histogram values, firstly by a factor of N_{conf} , secondly by a factor of the volume of the spherical shell corresponding to the separation between the particles and thirdly by an appropriate power of the pair excluded volume (i.e. the square for the first-order term and the cube for the second-order term). Errors may be estimated in the standard way, by dividing the total number of configurations into sub-batches and calculating sub-averages.

We used 1.6×10^9 trial chain configurations to obtain the first bridge diagram and 1.1×10^9 trial chain configurations to obtain the second bridge diagram. The relative error estimate is close to 1% except for the $r < 0.1b$ domain that is sampled poorly by this method.

In summary we now have four sets of integral equation results with which to compare simulation, corresponding to the four closures of Eqs. (6), namely PY, HNC, HNC+B2 (first-order bridge) and HNC+B3 (first- and second-order bridges).

V. RESULTS

A. Equation of state and stability with the bridge diagrams

The angular coefficients of the direct and the indirect correlation functions obtained from PY and HNC integral equations for non-spherical particles have already been extensively compared with simulation results in Refs. [20, 21, 27]. We limit our discussion to the effect

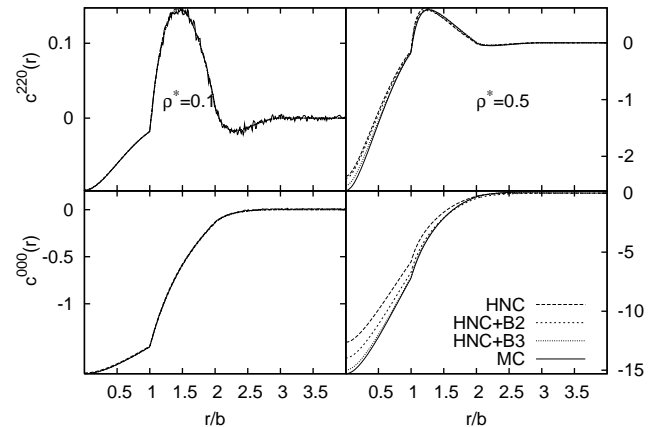


FIG. 1: The direct correlation function components 000 and 220 (in the lab frame) at reduced densities $\rho^* = 0.1$ (left) and $\rho^* = 0.5$ (right) obtained from IET and MC.

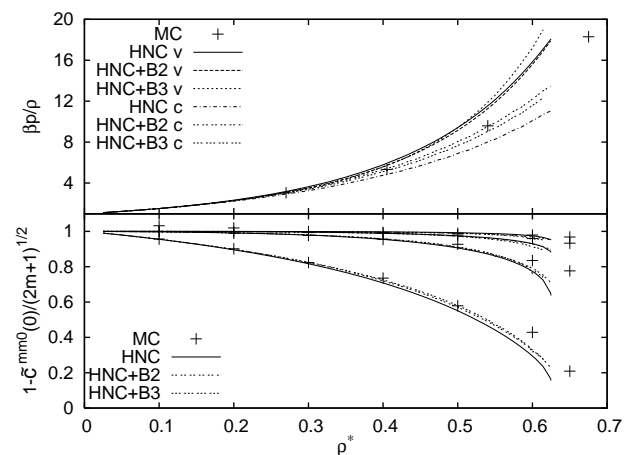


FIG. 2: The equation of state (upper panel) obtained by the virial (v) and compressibility (c) routes; and the Kerr coefficients (lower panel) obtained from pure HNC equation and HNC with the first two bridge diagram corrections. The lines for the Kerr coefficients correspond to $m = 2, 4, 6, 8$ in ascending order and the symbols represent the MC data (equation of state data from Ref. [23].)

of the inclusion of the bridge diagrams in the closure. Fig. 1, for two angular components of the direct correlation function at two densities, shows that the agreement between MC data and IET improves at high density if the HNC closure is supplemented by the inclusion of the low-order bridge diagrams.

We have a mixed picture for the equation of state and Kerr or stability coefficients. The latter gives a measure the stability of the isotropic phase relative to the nematic phase. The isotropic phase is stable when [47, 48]

$$1 - (2m + 1)^{-1/2} \bar{c}^{mm0}(0) > 0, \quad m = 2, 4, 6, \dots \quad (31)$$

where $\bar{c}^{mm0}(0)$ is the low- k limit of the Fourier-transformed direct correlation function component

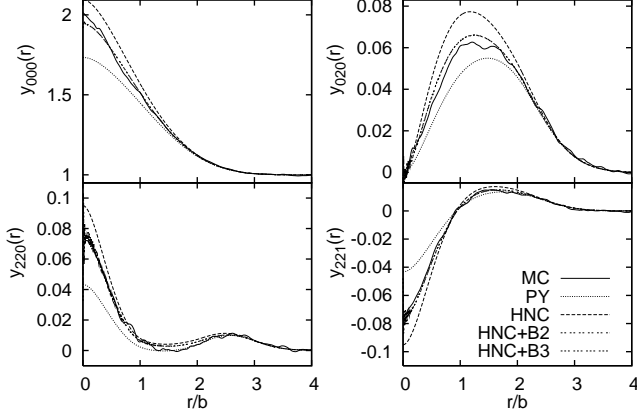


FIG. 3: The components of the y function at density $\rho^* = 0.1$ obtained from MC and IET: PY, HNC, HNC+B2 and HNC+B3.

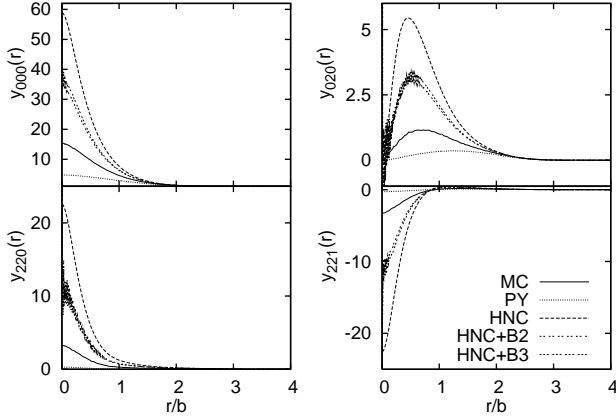


FIG. 4: The same functions as in Fig. 3 at density $\rho^* = 0.3$.

$c^{mm0}(r)$ in the laboratory frame. Fig. 2 shows that the inclusion of the first-order bridge diagram improves the agreement with the MC data for both the virial and compressibility pressures; the compressibility pressure, in particular, follows the MC results very closely. Surprisingly, the inclusion of the second-order bridge diagram increases the deviation of the pressure from MC at high densities. The same figure shows that the $m = 2$ Kerr coefficient agrees more closely with the simulation results if bridge corrections are included, but the change is less clear for $m > 2$.

B. Cavity correlation function

Before presenting our numerical results, it is worth considering some exact, analytical properties of the cavity function at $r = 0$. Firstly we note that at $r = 0$, the cavity function only depends on the relative orientations

of the two particles, 1 and 2, and thus may be expanded in terms of Legendre functions of $\mathbf{u}_1 \cdot \mathbf{u}_2$. Using the spherical harmonic addition theorem and comparing the results with Eq. (18), one finds that $y_{mn\chi}(0)$ is zero unless $m = n$. Furthermore $y_{mm\chi}(0) = (-)^{\chi} y_{mm0}(0)$. It may be seen from the figures that our calculated functions obey this condition to within statistical error. These properties result from the fact that the cavity function is well-behaved at $r = 0$ and similar conditions exist for the components of the direct correlation function and bridge function at $r = 0$.

Secondly we note that it has been shown for hard spheres that the cavity function at $r = 0$ is related to the excess chemical potential of the fluid, whilst the gradient of the cavity function at $r = 0$ is related to the pressure [35, 36]. These calculations may be generalised for anisotropic hard bodies and we obtain the exact results (for axially symmetric particles)

$$y(\mathbf{u}, \mathbf{u}, r = 0) = \exp(\beta\mu_{\text{ex}}) \quad (32)$$

$$\left. \frac{dy(\mathbf{u}, \mathbf{u}, r)}{dr} \right|_{r=0} = -\frac{1}{4\pi} \rho y(\mathbf{u}, \mathbf{u}, 0) \int_{u_{1,z} \geq 0} d\mathbf{u}_1 u_{1,z} \int d\mathbf{u}_2 r_c^2(\mathbf{u}_1, \mathbf{u}_2) g(r_c, \mathbf{u}_1, \mathbf{u}_2), \quad (33)$$

where the integral over \mathbf{u}_1 is restricted to the positive region of its z component; $r_c(\mathbf{u}_1, \mathbf{u}_2)$ is the contact distance of the two ellipsoids and $g(r_c, \mathbf{u}_1, \mathbf{u}_2)$ is the contact value of the pair distribution function at the given orientation. In the special case of hard spheres (i.e. $r_c = \text{constant}$), Eq. (33) gives the aforementioned relationship with the pressure, but in general, so far as we can see, there is no simple connection between the r.h.s. of Eq. (33) and any thermodynamic property of the fluid.

We now turn to our numerical results. Selected spherical harmonics components of $y(1, 2)$ are shown in Figs. 3-4 for two densities $\rho^* = 0.1, 0.3$. The most obvious conclusion is that both the PY and HNC predictions differ greatly from the simulation results as the density increases. In general the PY predictions are far too small in magnitude, whereas the HNC results are far too big. This is particularly evident for the isotropic component, $y_{000}(r)$, at low values of r , where $y_{000}(r)$ rises dramatically. At higher densities HNC and simulation coefficients differ by several orders of magnitude (from simulation $y_{000}(0) = 2050.1$, while from HNC theory $y_{000}(0) = 3033586.2$ for $\rho^* = 0.50$).

The inclusion of the bridge diagrams in the HNC closure improves significantly the agreement with MC at $\rho = 0.1$, see Fig. 3, but theory is still far from simulation for $\rho = 0.3$, see Fig. 4.

C. Bridge function

Shown in Figs. 5-7 are selected bridge function components calculated from simulation, PY and virial expansion.

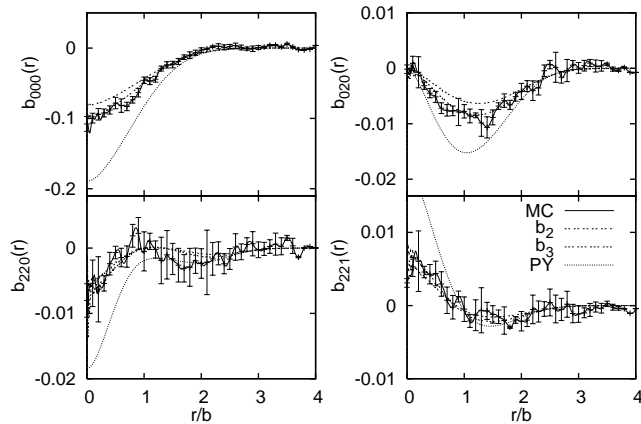


FIG. 5: Spherical harmonics components of $b(1,2)$ for $\rho^* = 0.10$ found from simulation, PY theory, and the virial expansion truncated at 2nd (b_2) and 3rd order (b_3).

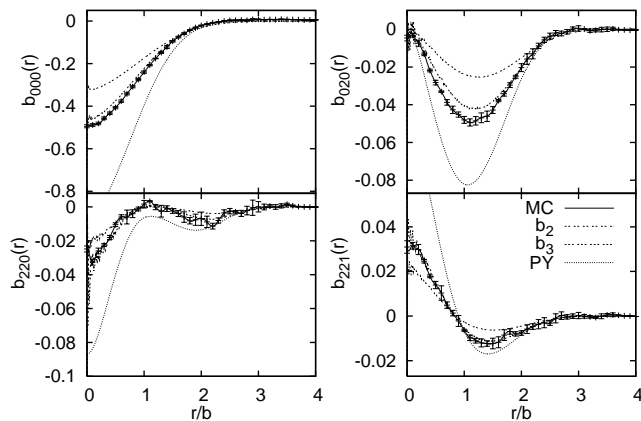


FIG. 6: $\rho^* = 0.2$ with same functions as in Fig. 5.

sion truncated at the second order ($b_2(1,2)$) and third order ($b_3(1,3)$).

As can be seen the PY $b_{000}(r)$ is always larger than the simulation $b_{000}(r)$ by approximately a factor of two. This seems to be independent of density. The shape of this component, both from simulation and PY theory, is similar to that of $b(r)$ calculated for simple fluids [6, 7]. The slope of $b_{000}(r)$ goes toward 0 as r goes to 0. This is similar to the behaviour seen for $b(r)$ for Lennard-Jones and soft sphere systems [6, 7], while for the HS fluid $b(r)$ approaches $r = 0$ almost linearly [49]. PY theory similarly overestimates the angular $b_{mn\chi}(r)$ coefficients.

Shown in Figs. 5-7 are also the bridge function calculated from simulation and from the first and second terms in the diagrammatic expansion. As can be seen at the lowest density studied ($\rho^* = 0.10$) the first-order expansion gives reasonable agreement with the simulated bridge function components, although they are underestimated relative to simulation. Adding the second term in

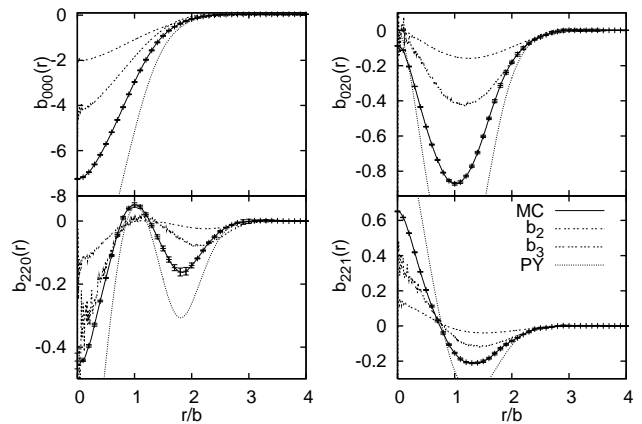


FIG. 7: $\rho^* = 0.5$ with same functions as in Fig. 5.

the expansion improves the agreement quite considerably. At a higher density, $\rho^* = 0.20$, the agreement is less good, with the first-order expansion seriously underestimating the coefficients. Again the agreement improves with the addition of the second term, in fact this diagrammatic approximation of the bridge function is better overall than the approximation obtained from the PY equation. As the density increases the agreement between MC results and the truncated virial expansion worsens, see Fig. 7.

VI. CONCLUSIONS

In this paper we have presented the calculation of the pair correlation functions $h(1,2)$, $c(1,2)$, $y(1,2)$, and $b(1,2)$ for the spheroid fluid from both simulation and IET. The total and direct correlation functions have been calculated using methods previously described [14, 20]. The cavity function was calculated from simulation using a combination of a direct simulation method and a test-particle approach. In order to improve the sampling of $y(1,2)$ in the direct simulation approach an umbrella sampling scheme using a weight function determined iteratively during the simulation itself is employed. From IET the cavity function is determined directly using the approximate closure relations.

Comparison between simulation and integral equation show, as reported before [20, 21, 27], reasonable agreement between the coefficients of the total and direct correlation functions. However theory predicts the simulated cavity function poorly, with PY theory underestimating and HNC theory overestimating $y(1,2)$ within the overlap region. This error rapidly increases with density, leading to, at the highest densities studied, errors of several orders of magnitude.

The bridge function calculated from the truncated virial expansion is in good agreement with MC results at low density but significant differences appear as the density increases. The bridge function calculated from

PY theory follows the general shape of the MC results but the quantitative agreement is poor.

To the best of our knowledge this work presents the first calculation of both the full bridge and cavity functions for molecular fluids from simulation. As the approximate closure relations used in integral equation theory correspond to approximations to the bridge function, knowledge of its exact form will, hopefully, be of great benefit in developing improved theories of molecular fluids.

Acknowledgements

LA and AJM thanks Aurelian Perera for useful discussions on integral equation numerical techniques. This work was supported by EPSRC grants GR/S77240 and GR/S77103 Computational resources were provided by the Centre for Scientific Computing, University of Warwick and Manchester Computing, University of Manchester.

APPENDIX: WANG-LANDAU SAMPLING

Consider a system with a property X . The probability of finding the system with a particular $X = X_1$ is given by a probability distribution $p(X)$. In many cases this distribution is peaked around certain values of X , meaning that in a standard simulation values away from these are likely to be poorly sampled. When it is desirable to get information about these unlikely states it is common to apply a weight function, $g(X) = \exp(-\beta W(X))$, that changes the standard Metropolis acceptance criteria to

$$p(X_1 \rightarrow X_2) = \frac{g(X_1)}{g(X_2)} \exp[-\beta(E(X_2) - E(X_1))] . \quad (\text{A.1})$$

The simulated probability distribution $p_{\text{sim}}(X)$ then becomes

$$p_{\text{sim}}(X) = p(X)g(X). \quad (\text{A.2})$$

Ideally the effect of the weight function is to make the simulation probability distribution flat, i.e. $p_{\text{sim}}(X) = 1$, which implies

$$W(X) = \frac{1}{\beta} \log p(X), \quad (\text{A.3})$$

Of course the $W(X)$ needed to achieve this perfectly flat histogram is not known in advance, otherwise the probability distribution would also be known in advance, thus rendering the actual act of performing the simulation somewhat redundant. The problem has then become one of determining the weight function needed to produce a flat histogram.

At the start of the simulation the weight function is initially set to be constant, i.e. $g(X) = 1, W(X) = 0$.

After each attempted MC move $X_1 \rightarrow X_2$ (made using the modified criteria Eq. A.1) the weight function for the resulting state $X_{1/2}$ (either X_1 or X_2) is multiplied by a modification factor,

$$\begin{aligned} g(X_{1/2}) &\rightarrow f g(X_{1/2}) \\ W(X_{1/2}) &\rightarrow W(X_{1/2}) + \log f . \end{aligned}$$

Simultaneously the probability histogram $p_{\text{sim}}(X_{1/2})$ is also incremented. This continues with the weight function and probability being updated after every attempted change in X until probability histogram is flat. The flatness condition may be defined in several ways and will be discussed momentarily. Once this condition has been reached the probability histogram is reset to zero and f is modified. Typically

$$\begin{aligned} f &\rightarrow \sqrt{f} \\ \log f &\rightarrow \frac{1}{2} \log f . \end{aligned}$$

This then continues until the modification factor becomes close to 1 ($\log f$ gets close to machine precision). The final $p(X)$ may then be determined from

$$p(X) = p_{\text{sim}}(X)/g(X) = p_{\text{sim}}(X) \exp(\beta W(X)) . \quad (\text{A.4})$$

A few general notes on the method are due. First updating the weight function during the simulation may be seen to violate the principle of detailed balance. However, this is most severe at the beginning of the simulation. As f tends toward 1, the changes in the weight function become increasingly small. It has been shown that a viable MC scheme need only asymptotically obey detailed balance [50]. Additionally once a sufficiently good weight function has been determined, the simulation may be continued without updating the weight function and statistics may be gathered from this [41]. Secondly as a perfectly flat histogram is unlikely to be reached during a finite simulation the flatness condition may be seen to be somewhat arbitrary. In the first implementations the histogram was declared flat when the smallest $p_{\text{sim}}(X)$ was within a given percentage of the average. However it is not impossible to imagine pathological distribution (e.g. with a few large narrow peaks) that are far from flat but still fulfil this criteria. An alternative is to update f whenever every bin has been visited a minimum number of times. While this may appear less rigorous than the first method, as the simulation progresses and $W(X)$ becomes closer to $(1/\beta) \log p(X)$ then $p_{\text{sim}}(X)$ should become flat. Additionally this ensures that $p_{\text{sim}}(X)$ has a chance to adjust to the new f and avoids any spurious early updates. One final point is that the Wang-Landau method was originally formulated for systems with discrete degrees of freedom (specifically the Ising model). When X is continuous the probability histogram and weight functions are calculated for bins of finite width X , $X + \delta X$ and bin width may become a perturbing factor in the results.

In the present problem we are interested in the probability distribution of a pair of non-interacting particles. The variable of interest is the radial separation of these particles r_{12} , which is discretized into bins of width $\delta r = 0.01$. As mentioned before the r_{12} range is divided into a set of overlapping windows. A Wang-Landau sim-

ulation is used to determine the weight function to produce a constant $p(r_{12})$ within each window. f is updated whenever $p(r_{12})$ fulfils two criteria: i) the largest difference between any bin and the average is less than 10% and ii) the smallest values of any bin is 100.

-
- [1] J.-P. Hansen and I. R. McDonald, *Theory of Simple Liquids* (Academic Press, London, 1986), 2nd ed.
 - [2] C. G. Gray and K. E. Gubbins, *Theory of molecular fluids. 1. Fundamentals* (Clarendon Press, Oxford, 1984).
 - [3] R. D. Groot, J. P. van der Eerden, and N. M. Faber, J. Chem. Phys. **87**, 2263 (1987).
 - [4] G. Torrie and G. N. Patey, Molec. Phys. **34**, 1623 (1977).
 - [5] J. A. Ballance and R. J. Speedy, Molec. Phys. **54**, 1035 (1985).
 - [6] M. Llano-Restrepo and W. G. Chapman, J. Chem. Phys. **97**, 2046 (1992).
 - [7] M. Llano-Restrepo and W. G. Chapman, J. Chem. Phys. **100**, 5139 (1994).
 - [8] J. Kolafa, S. Labík, and A. Malijevský, Molec. Phys. **100**, 2629 (2002).
 - [9] F. J. Rogers and D. A. Young, Phys. Rev. A **30**, 999 (1984).
 - [10] G. Zerah and J.-P. Hansen, J. Chem. Phys. **84**, 2336 (1986).
 - [11] Y. Rosenfeld and N. W. Ashcroft, Phys. Rev. A **20**, 1208 (1979).
 - [12] P. Attard and G. N. Patey, J. Chem. Phys. **92**, 4970 (1989).
 - [13] S. Rast, P. H. Fries, and H. Krienke, Molec. Phys. **96**, 1543 (1999).
 - [14] M. P. Allen, C. P. Mason, E. de Miguel, and J. Stelzer, Phys. Rev. E **52**, R25 (1995).
 - [15] L. Lue and D. Blankschtein, J. Chem. Phys. **102**, 5427 (1995).
 - [16] Y. Duda, L. L. Lee, Y. Kalyuzhnyi, W. G. Chapman, and P. D. Ting, Chem. Phys. Lett. **339**, 89 (2001).
 - [17] Y. Duda, L. L. Lee, Y. Kalyuzhnyi, W. G. Chapman, and P. D. Ting, J. Chem. Phys. **114**, 8484 (2001).
 - [18] J. Sedlbauer, S. Labík, and A. Malijevský, Phys. Rev. E **49**, 3179 (1994).
 - [19] P. H. Fries and G. N. Patey, J. Chem. Phys. **82**, 429 (1985).
 - [20] A. Perera, P. G. Kusalik, and G. N. Patey, J. Chem. Phys. **87**, 1295 (1987).
 - [21] A. Perera and G. N. Patey, J. Chem. Phys. **89**, 5861 (1988).
 - [22] M. Letz and A. Latz, Phys. Rev. E **60**, 5865 (1999).
 - [23] R. Pospíšil, A. Malijevský, and W. R. Smith, Molec. Phys. **79**, 1011 (1993).
 - [24] R. C. Singh, J. Ram, and Y. Singh, Phys. Rev. E **54**, 977 (1996).
 - [25] L. Blum and A. J. Torruella, J. Chem. Phys. **56**, 303 (1972).
 - [26] L. Blum, J. Chem. Phys. **57**, 1862 (1972).
 - [27] J. Talbot, A. Perera, and G. N. Patey, Molec. Phys. **70**, 285 (1990).
 - [28] S. Labík, A. Malijevský, R. Pospíšil, and W. R. Smith, Molec. Phys. **74**, 261 (1991).
 - [29] J. Ram, R. C. Singh, and Y. Singh, Phys. Rev. E **49**, 5117 (1994).
 - [30] M. Kinoshita and M. Harada, Molec. Phys. **74**, 443 (1991).
 - [31] K.-C. Ng, J. Chem. Phys. **61**, 2680 (1974).
 - [32] W. B. Streett and D. J. Tildesley, Proc. R. Soc. Lond. A **348**, 485 (1976).
 - [33] L. Blum and D. Henderson, J. Chem. Phys. **74**, 1902 (1981).
 - [34] L. Blum, P. T. Cummings, and R. Bratko, J. Chem. Phys. **92**, 3741 (1990).
 - [35] J. R. Henderson, Molec. Phys. **48**, 389 (1983).
 - [36] E. Meeron and A. J. F. Siegert, J. Chem. Phys. **48**, 3139 (1968).
 - [37] D. Frenkel and B. Smit, *Understanding molecular simulation : from algorithms to applications* (Academic Press, San Diego, 2002), 2nd ed.
 - [38] A. M. Ferrenberg and R. H. Swendsen, Phys. Rev. Lett. **63**, 1195 (1989).
 - [39] F. Wang and D. P. Landau, Phys. Rev. E **64**, 056101 (2001).
 - [40] M. S. Shell, P. G. Debenedetti, and A. Z. Panagiotopoulos, Phys. Rev. E **66**, 056703 (2002).
 - [41] E. B. Kim, R. Faller, Q. Yan, N. L. Abbot, and J. J. de Pablo, J. Chem. Phys. **117**, 7781 (2002).
 - [42] N. Rathore, Q. Yan, and J. J. de Pablo, J. Chem. Phys. **120**, 5781 (2004).
 - [43] W. H. Press, B. P. Flannery, S. A. Teukolsky, and W. T. Vetterling, *Numerical Recipes in Fortran* (Cambridge University Press, Cambridge, 1992), 2nd ed.
 - [44] M. P. Allen, G. T. Evans, D. Frenkel, and B. M. Mulder, Adv. Chem. Phys. **86**, 1 (1993), and references therein.
 - [45] F. H. Ree and W. G. Hoover, J. Chem. Phys. **40**, 939 (1964).
 - [46] F. H. Ree and W. G. Hoover, J. Chem. Phys. **46**, 4181 (1967).
 - [47] J. Stecki and A. Kloczkowski, Journal de Physique **40**, C3 (1979).
 - [48] J. Stecki and A. Kloczkowski, Molec. Phys. **42**, 51 (1981).
 - [49] D. Henderson and S. Sokolowski, J. Chem. Phys. **103**, 7541 (1995).
 - [50] D. J. Earl and M. W. Deem, J. Phys. Chem. B **109**, 6701 (2005).